Polar-angle representation of saccadic eye movements in human superior colliculus

Ricky R. Savjani[a,b,c], **Sucharit Katyal**[d], **Elizabeth Halfen**[a,b], **Jung Hwan Kim**[a,b], **David Ress**[a,b,d,*]

[a]Department of Neuroscience, Baylor College of Medicine, Houston, TX 77030, USA

[b]Core for Advanced Magnet Resonance Imaging, Baylor College of Medicine, Houston, TX 77030, USA

[c]Texas A&M Health Science Center College of Medicine, Bryan, TX 77807, USA

[d]Departments of Neuroscience and Psychology, The University of Texas at Austin, 78712, USA

Abstract

The superior colliculus (SC) is a layered midbrain structure involved in directing both head and eye movements and coordinating visual attention. Although a retinotopic organization for the mediation of saccadic eye-movements has been shown in monkey SC, in human SC the topography of saccades has not been confirmed. Here, a novel experimental paradigm was performed by five participants (one female) while high-resolution (1.2-mm) functional magnetic resonance imaging was used to measure activity evoked by saccadic eye movements within human SC. Results provide three critical observations about the topography of the SC: (1) saccades along the superior-inferior visual axis are mapped across the medial-lateral anatomy of the SC; (2) the saccadic eye-movement representation is in register with the retinotopic organization of visual stimulation; and (3) activity evoked by saccades occurs deeper within SC than that evoked by visual stimulation. These approaches lay the foundation for studying the organization of human subcortical – and enhanced cortical mapping – of eye-movement mechanisms.

Keywords

Superior colliculus; Saccades; fMRI; Subcortical vision; Topography; Attention

Introduction

The superior colliculus (SC) is a layered midbrain nucleus with multiple functions including processing vision, orienting attention, priming head movements, generating saccadic eye movements and integrating multiple sensory inputs. The SC is organized into seven laminae

of distinct cytoarchitecture with alternating cellular and fiber character. There are three superficial layers and four inner layers (Wurtz and Albano, 1980). The superficial layers receive direct retinal input and contain visual neurons with retinotopically organized receptive fields (Cynader and Berman, 1972; Feldon and Kruger, 1970). The inner layers are separated into intermediate and deep layers. The two intermediate layers contain motor output neurons that control eye movements (Robinson, 1972), whereas the two deep layers contain multisensory integration neurons (Meredith and Stein, 1990; Sprague and Meikle, 1965).

The oculomotor function of the SC was first discovered by electrical stimulation (Adamuk, 1872; Donders, 1872), and later induced via strychnine (Apter, 1946) in anesthetized cats. Extensive studies in alert monkeys via electrical stimulation (Robinson, 1972), neuronal recordings (Mohler and Wurtz, 1976), and lesions (Wurtz and Goldberg, 1972) then characterized the non-human primate topography of the SC [see several reviews (Fuchs et al., 1985; Sparks and Hartwich-Young, 1989; Sparks and Jay, 1986; Wurtz and Albano, 1980):]. The intermediate layers of monkey SC contain a retinotopically organized saccadic eye-movement map (Schiller and Stryker, 1972). Saccade magnitude is roughly mapped along the rostral-caudal axis of monkey SC, whereas saccade direction is mapped along the medial-lateral axis of the SC. The mapping is not linear, with over-representation of small-magnitude saccades, and of polar angles close to the horizontal meridian (Sparks et al., 1976). Also, the SC topography shows a small but variable amount of tilt in the left-right direction that is in rough correspondence to the anatomic tilt of the colliculi relative to the neuraxis (Robinson, 1972). Recent studies have further revealed that the upper visual field is over-represented, comprised of smaller and more sensitive receptive fields (Hafed and Chen, 2016).

In humans, studies to infer SC function have historically been restricted to whole-brain functional magnetic resonance imaging (fMRI). Whole-brain or low-resolution (i.e., 2-mm voxels) fMRI has documented saccade-related activity in SC (de Weijer et al., 2010; Furlan et al., 2015; Krebs et al., 2010), and reach-related functions performed by the deep layers of SC (Himmelbach et al., 2013). However, the low-resolution measurements did not delineate the detailed topography of SC functions. Further, previous human studies of saccadic mapping in cortex, not SC, have attempted to use fMRI phase-encoding approaches (Connolly et al., 2015; Konen and Kastner, 2008; Schluppeck et al., 2005; Sereno et al., 2001) but with two critical limitations: (1) a very low duty cycle and (2) reverse saccades made immediately after forward saccades. The low duty cycle forces participants to fixate most of the time instead of performing saccades, which reduces the evoked hemodynamic activity. A paradigm with a higher duty cycle that isolates saccades in one direction is likely to be crucial to getting reliable SC topography measurements with fMRI.

More recent human fMRI studies were able to demonstrate the presence of visual stimulation retinotopy (Schneider and Kastner, 2005), and covert attention signals (Schneider and Kastner, 2009) in superficial SC using higher resolution fMRI (1.5×1.5 x 2-mm voxels) targeted specifically to midbrain. Our laboratory expanded upon these studies using higher resolution fMRI (1.2-mm cubic voxels) to demonstrate a detailed transverse

retinotopic organization of visual attention and stimulation upon SC (Katyal et al., 2012, 2010; Katyal and Ress, 2014).

Here, we improved those methods and developed a novel task to measure the polar angle representation of saccadic eye movements, elucidating their topography within human SC. Using our previous visual stimulation paradigm optimized for human fMRI in SC (Katyal et al., 2010), we show that these eye movement maps are in register with the retinotopy observed in SC superficial layers. Finally, we demonstrate that the measured activity is elicited from the intermediate layers. Altogether, our results again confirm macaque electrophysiology, and create an experimental framework for further experiments in human eye-movement physiology both in brainstem and cortex.

Materials and methods

Participants

We recruited five participants (4 males, all right-handed) to undergo several ~2 h long scanning sessions. One-to-two sessions were acquired for each participant to discern the polar-angle representation of leftward and rightward saccadic eye movements separately, which were expected to evoke activity primarily in the contralateral SC. Each eye-movement session consisted of 12–16 278-s runs. One-to-two scanning sessions were also acquired from each participant for visual stimulation retinotopic mapping. Visual stimulation experiments were intended to evoke activity in both SC since the entire visual field was stimulated in a single session. Retinotopy sessions consisted of 14–16 228-s runs. Participants gave informed consent prior to scanning based on our approved protocol from the Baylor College of Medicine Institutional Review Board.

Experimental design

Stimuli were generated using MATLAB R2015a (Mathworks, Natick, MA) and PyschToolbox-3 (Brainard, 1997). Stimuli were presented on a 32" LCD BOLD Screen (Cambridge Research Systems, Kent, UK) at the back of the scanner bore 1.3 m away from the participants' eyes. The display was gamma corrected using an i1 Pro 2 spectrophotometer (X-Rite, Grand Rapids, MI), and had a mean luminance of 305 cd/m^2.

We designed a paradigm in which participants performed many saccades in one direction while minimizing saccades in the opposing direction (see Movie M1). Participants made saccades either to the left or to the right (activating primarily the contralateral SC) while we cyclically varied the vertical component of the saccade to correspond to the lower, horizontal, and upper visual field (Fig. 1). Participants performed three 6° saccades guided by a green dot target in a static grid of 12 red dots. The static red dots were arranged as 4 dots separated by 6° along each of the three principle axes (horizontal, 45° diagonal, and −45° diagonal). The use of a static grid reduced differential contrast effects from retinal slip. Although each saccade and subsequent pursuit produces motional stimulation, the shape of the static grid minimizes differential effects of this stimulation between angular conditions. The use of green-red color contrast minimized the effects of bottom-up color contrast in target discrimination. Further, human SC has recently been shown to adapt to red-green

contrast (Chang et al., 2016), so our static red-green grid reduces cue-evoked visual stimulation during saccadic eye movement measurements.

Supplementary video related to this article can be found at https://doi.org/10.1016/j.neuroimage.2017.12.080

Participants initially held fixation at an upper corner of the display. The first saccade was initiated when an adjacent red dot turned green to indicate the saccade target. Once the saccade was made, participants had to discriminate between the outlines of two possible shapes (circle or square) presented within the target dot. This required visual attention to be engaged and saccades to be made more reliably. Participants responded via button press, which triggered the green dot to appear at the next target along the current axis. After three saccades, the participants then performed a smooth pursuit (1.2 s) back to the first dot. Saccades and the pursuit were continued along the same axis for 9.6 s, and then participants performed another smooth pursuit to the start of the next axis. The discrimination task had to be performed 0–2 random times (truncated Poisson distribution, $\lambda = 1$) during each 1.2-s smooth pursuit, encouraging attention to remain engaged and eye movements to be restrained to the pursuit path. Participants performed 9 cycles in a single run (~4.5 min) and ~15 runs per session. Leftward and rightward saccades were run on separate sessions to measure the contralateral response of each SC independently.

Retinotopic maps were also acquired for all 5 participants using our previous phase-encoded visual stimulation paradigm (Katyal et al., 2010). Participants fixated at the center of the display while a wedge (90° polar angle) of moving dots rotated around the entire polar angle to measure retinotopy for both superior colliculi in a single session. The rotating wedge consisted of 6 virtual sectors, and in one sector, the dots were moving either faster or slower than all other sectors. Participants performed a speed discrimination task every 2 s. The speed difference was adjusted using a staircase design to control task difficulty and engage attention, boosting signal levels for the retinotopy measurement.

Saccadic eye movements

Eye movement were measured with the SR EyeLink 1000 Plus (Scientific Research, Ontario, Canada) both outside of the scanner during training sessions and inside the scanner during fMRI acquisition. Inside the scanner, the infrared light and camera were placed beneath the LCD display and angled at the head-coil mounted mirror allowing us to track the participant's right eye at ~130cm lens-to-eye distance. Raw (x, y) position coordinates were sampled at 1000 Hz. Saccade reports were generated using the EyeLink Data Viewer (Scientific Research, Ontario, Canada) and further analyzed in MATLAB. Saccades were detected using three minimum thresholds: position (>0.15°), velocity (>30°/s), and acceleration (>9500°/s^2). Eye blinks were detected when the pupil diameter was too small (<1 mm), obstructed, or not tracked, and any saccades during blinks were discarded from analysis. Polar plots were created to visualize the saccades, where polar angle represented the direction of a saccade and eccentricity represented the amplitude of a saccade, which was also plotted in a histogram. Smooth pursuits and correction eye movements were further distinguished from saccades by restricting saccade analysis to eye movements towards the

cued horizontal visual field (i.e., left or right) and eye movements with amplitudes greater than 1° visual angle.

MRI methods

Imaging was conducted on a Siemens (Erlangen, Germany) 3T Magnetom Trio scanner at the Core for Advanced Magnetic Resonance Imaging (CAMRI) at Baylor College of Medicine. Eight 1.2-mm-thick quasiaxial slices (170-mm field of view) covered the entire SC with the prescription oriented roughly perpendicular to the local neuraxis. Functional data were acquired using a 3-shot spiral (Glover, 1999; Glover and Lai, 1998) dual-echo (both outward) sequence (Li and Glover, 2006) that has been shown to boost functional SNR by >50% compared to single-echo methods (Singh et al., 2017). We used $T_R = 0.8$ s for each shot, yielding a 2.4-s volume-acquisition time for our 3-shots. To obtain best contrast, T_E was set to 25 ms for the first echo, and acquisition time for each echo was 34 ms, giving an effective echo time of 59 ms for the second echo. The dual echoes were combined as a signal-weighted average.

A set of T_1-weighted structural images was obtained on the same prescription at the end of the session using a three-dimensional (3D) fast low-angle shot (FLASH) sequence (minimum TE and TR, 15° flip angle, 0.9-mm inplane pixel size) (Fig. 2B). These images were used to align the functional data to the segmented structural reference volume. A high-resolution (0.7-mm cubic voxels) T1-weighted structural volume anatomy was obtained for each participant in a separate session, using an MP-RAGE sequence (TR = 2600 ms, minimum TE, TI = 1100 ms, flip angle = 9°, 3 averages, 24-min acquisition time).

Data analysis

Preprocessing—Image analysis was conducted using the mrVista software package (http://web.stanford.edu/group/vista/cgi-bin/wiki/index.php/MrVista) and a host of custom modifications designed to enable high spatial resolution sub-cortical imaging. In particular, we incorporated our sub-cortical depth-mapping procedures (Khan et al., 2011), utilized an inverted form of tissue mesh definition (analogous to gray-matter mesh definition), and a corresponding inverted form of surface-mesh visualization useful for sub-cortical structures. Moreover, a framework was added to deal with the use of multi-echo fMRI data. The first 12 s of each retinotopy run were discarded to remove transient effects. Similarly, the first 19.2s of each eye movement run were discarded to remove transients and to allow participants to become accustomed to the eye-movement task. The following preprocessing was conducted on each of the two echoes for all runs (visual stimulation and eye movement), analogous to our previous pipeline (Katyal et al., 2010): slice-timing correction (zeroed to task onset) and intensity-based motion compensation using a robust algorithm (Nestares and Heeger, 2000). Motion compensation information was obtained only from the first echo because of its higher SNR; these data were then applied to both echoes. The two processed echoes were then combined as a signal-weighted average. Finally, baseline trend removal was performed using a high-pass filtering approach.

Surface analysis—For each participant, we collected a high-resolution (0.7-mm isovoxel) structural volume in separate runs. We used this structural volume to segment their

brainstem (including portions of the thalamus) via a combination of automatic (e.g., active contour evolution) and manual approaches in ITK-SNAP (Yushkevich et al., 2006) (Fig. 2A). Two participants' brains were initially segmented using the newer Bayesian approaches in FreeSurfer 6.0 (Iglesias et al., 2015), followed by manual editing. A surface model was built at the tissue-cerebrospinal fluid interface using a deformable surface algorithm (Xu et al., 2006). Functional data (Fig. 2B) were then spatially aligned and resampled to the high-resolution structural volume, averaged across runs, and visualized on the surface. Distance along the surface, d_{mesh}, was estimated by summing Euclidean distances along the mesh from a reference point on each participant's inter-collicular axis. A Euclidean nearest-neighbor distance map was also computed from SC tissue voxels to the vertices of the surface to give a measure of the depth (s, mm) of the tissue voxels (Khan et al., 2011; Ress et al., 2007). Time-series data were averaged over a particular range of depth values to improve signal-to-noise ratio (SNR).

Phase mapping—A sinusoid at the stimulus repetition frequency (24 s for visual stimulation data, 28.8 s for eye movement data) was fit to the depth-averaged data (0–1.6 mm for visual stimulation data, 0.6–1.8 mm for eye-movement data) using coherence analysis. These fits provide three parameters: amplitude, phase, and coherence. Amplitude measures the strength of the evoked activation, phase measures the time delay of the response, and coherence is equivalent to the Pearson's correlation coefficient, quantifying the fraction of variance explained by the sinusoidal fit. The phase, specifically, is used to measure the relationship of the fMRI response to the current state of the stimulus (visual stimulus polar angle or saccade angle). Phase maps, expressed in units of time delay, were projected onto the brainstem surface to visualize the topography of visual stimulation and eye movements.

Region-of-interest (ROI) generation—We generated elliptical ROIs to demarcate the phasic progressions of saccade-evoked activity for quantitative analyses. Given that the task design utilized only a single amplitude saccade (6°) to drive the SC, we expected that phasic progressions representing saccadic activity would result only in narrow bands of activity representing the strongest signal emerging from the intermediate layers, unlike in our previous studies in which visual stimulation and attentional maps activated entire colliculi (Katyal et al., 2010). Further, the intermediate layers are more difficult to measure due to vascular noise sources and the decrease in SNR. As such, we developed an objective approach to delineate the most robust SC activity representing saccadic activity using a grid search initialized only by the putative angle in which the saccadic progression could be seen visually.

First, surface representations of the SC were flattened to form a 2D image (Wade et al., 2002; Wandell et al., 2000) (Fig. 2C). The phasic progression from medial to lateral was visually observed and then delineated with two vertices on the surface to define the start and stop of the putative eye movement maps; these two vertices were then transformed to the flat image. Next, many (~20,000) elliptical ROIs were generated upon the flattened image and each was transformed into the reference volume; note that this transformation creates a somewhat distorted version of the ellipse on the mesh (Fig. 2D). The many ellipses

corresponded to gridded variations in five parameters: size (15–60% of one whole SC area); aspect ratio (3.5–7); *x, y* center coordinates (each varied ±2 pixels from the midline of the delineated phase progression); and the elliptical angle (±15° relative to the angle of the delineated phase progression). An exhaustive search was then conducted to maximize five criteria: (1) number of activated (with a moderate threshold of $p < 0.2$) voxels, ν_{sig}; (2) geometric average p-value, $\bar{p}_{geom} = \sqrt[n]{\prod_{i=1}^{n} p}$; (3) phase range (defined by median absolute deviation), $\phi_{range} = \mathrm{median}(ph_i - \mathrm{median}(ph))$; (4) correlation (variance explained) of the linear fit between the mesh distance d_{mesh} and the phasic progression

$\phi, \sigma_{exp}^2 = 1 - \dfrac{var(\phi - d_{mesh})}{var(\phi)}$; and (5) the reciprocal deviation of the same linear fit and the expected progression across the collicular width, $\delta = 1/abs(ellipse_{slope} - target_{slope})$. The five optimization criteria were multiplied together to yield an overall metric,

$opt = \nu_{sig}\, \bar{p}_{geom}\, \phi_{range}\, \sigma_{exp}^2\, \delta$, for each ROI. The top four values of *opt* identified the best ROIs, which were examined visually for quality confirmation. The top fitting ROI was used for subsequent analyses.

Laminar profile analysis—We then examined the amplitude of the complex response as a function of laminar depth within the elliptical SC ROIs, similar to our previous approaches (Katyal et al., 2010, 2012; Katyal and Ress, 2014), using surface-based methods (Khan et al., 2011). Complex amplitude data were first averaged together across all runs for each participant. A phase normalization was performed to correct for the variable hemodynamic time delay across the ROI. Cylindrical volume elements (1.2-mm diameter) are formed normal to the surface mesh; these elements provide transverse averaging of the data that improves functional SNR. Within these elements, we obtained the amplitude-weighted mean phase. Complex amplitudes within each element were then projected upon this phase. After this projection across all elements within the ROI, a boxcar-smoothing kernel (1.2 mm width in bin steps of 0.1 mm) was convolved with the projected amplitude data as a function of depth to obtain the laminar profile. The laminar profiles for both eye movement and visual stimulation experiments were normalized by their peak amplitudes to enable comparisons and averaging across participants.

We used bootstrapping to obtain confidence intervals on the laminar amplitude profiles in each participant and all participants combined, for both visual stimulation and eye movement experiments. For each ROI, we calculated the complex amplitudes for each run. We then resampled across runs with replacement over 5000 iterations, and calculated the laminar profile anew for each resampled average. The 68% confidence intervals, equivalent to the standard-error-of-the-mean for normally distributed data, are shown by shading on laminar profile plots.

Depth values for the peaks of the laminar profiles were calculated to quantify comparisons of depth between the attention and stimulation conditions. The peak depths were also bootstrapped across the ensemble of runs to obtain confidence intervals and *p*-values for differences between peak depth values for visual stimulation and eye-movement maps.

Retinotopy-eye movement correlation—Within each optimal elliptical ROI for all participants, we measured the registration between phase maps for saccadic eye movements and visual stimulation. The raw eye-movement maps spanned the entire cycle (2π radians), and thus were converted to visual field coordinates in degrees. The phase progressions within the ROI were first scaled onto a range of 90°, then these data were centered around 0° for rightward saccades, and 180° for leftward saccades. Visual stimulation phase data were corrected by estimating the hemodynamic delay as the mean phase observed in significant (p < .05) voxels of each colliculus within the elliptical ROI, and this was then subtracted from the phase data. This procedure centers the data at 0° (right horizontal), so we add 180° for the left visual field (right colliculus).

We again used bootstrapping to obtain confidence intervals on the correlations for each participant and all participants combined. For each session, we calculated a run-by-run ensemble of depth-averaged complex amplitude datasets. We then performed our correlation analysis with the retinotopy data for 5000 averages of the attention-condition runs, each average obtained by resampling the ensemble with replacement. The *p*-values corresponded to the fraction of the correlations yielding a fit with slope >0.

Results

Eye movements

Before each saccade-mapping session, we trained all participants on 2–3 runs outside of the scanner and quantified the reliability of their eye movements (Fig. 3A). Saccades were detected and visualized on polar plots to show the eccentricity and polar angle of each saccade. Saccades were color coded to represent their cycle timing along the three polar angles of the task. We were also able to obtain reliable eye tracking in the scanner from two participants on both rightward and leftward eye-movement sessions (Fig. 3B). Histograms indicated eye movements were slightly hypermetric to the cued amplitude (6.29 ± 1.95°, shown in gray) in the cued direction (angular error: 0.82°± 10.01°). Long-tailed distributions in the opposite direction (white) were also observed. The task periods designed to evoke smooth pursuits often contained saccades of variable amplitude, but most were less than 3° (median: 0.8°, mean: 3.07°±3.19°). Small correction saccades also contribute to the opposite-direction saccades, as saccades to targets were often hypermetric, followed by a small saccade in the reverse direction. All participants performed reliably in both the discrimination task during the saccades (mean accuracy: 82.8 ± 8.6% across all sessions and participants) and the speed discrimination task during visual stimulation (mean accuracy: 70.3 ± 5.1%); see Fig. S2 for quantification of behavioral task performance.

The quality of the eye-tracking measurements appears much worse inside the scanner because of several issues. First, the eye-tracker inside the scanner must use longer-range optics (~1 meter) than outside the scanner (0.2 meter). This forces use of smaller numerical apertures, reducing light-collection efficiency and increasing noise levels and sensitivity to aberrations. Second, images of the eyes must be obtained through the eye-holes in the head coil, which further complicates the optics, and adds nuisance IR reflections that can confuse the analysis routines. Third, even when eye-tracking is initially well-calibrated inside the scanner, the quality of the eye-tracking often degrades over the course of a run as the

participant's head sinks into the foam padding, as the head vibrates from operation of the gradients, and as the head and body move from run to run. This variability can be reduced by performing re-calibration measurements between runs, but we elected not to perform these recalibrations as the scanning sessions were already long (~2 h). Finally, the long sessions within the confines of the scanner were far more demanding on participant eye-movement performance, so it is not surprising that their variability becomes larger.

Polar angle maps of saccadic eye movements

Saccades along the superior-inferior visual field were mapped along the medial-lateral axis of the SC in all 5 participants (Fig. 4). Our eye-movement task involved making $6°$ saccades toward one hemifield, with smooth pursuit in the opposite direction. Accordingly, we see organized phase progressions only in one contralateral SC at a time. We generated ROIs by using an objective optimization approach to demarcate the area of phase progression near the crown of the colliculus likely to represent the saccadic eye-movement topography. Within these ROIs, we found significant correlations of saccadic eye-movement phase with distance along the medial-lateral axis of the SC at the group level (slope: 0.451, $r = 0.734$, p ~ .0002, Fig. 5). Significant correlations ($p < .05$) were also observed in 7 out of 10 individual SCs (Fig. S3). Strong activity was also evident in many other portions of both contralateral and ipsi-lateral colliculi. In particular, several ipsilateral colliculi exhibit reversed phase progressions (S1L, S2L, S4L, S1R, S2R, S3R, and S4R) that were more rostral than the contralateral progressions. This rostral pole activation could represent activity from the smooth pursuits, but in our experience, the rostral pole is often contaminated with vascular nuisance activations, so these activations will not be further discussed. Also, participant saccades were not perfectly controlled, and reverse eye movements occurred in two ways. First, during the latter portions of the pursuit periods participants occasionally would predictively saccade to the endpoint of the pursuit (see Movie M1). Second, smaller amplitude opposite-direction correction saccades frequently occurred after hypermetric forward saccades. The erratic nature of these poorly controlled eye movements likely contributed to the poorly organized activation on the ipsilateral colliculus.

Weak but significant activation was also observed in early visual cortical areas V1—3 (Fig. S4). However, this activity had a biphasic rather than triphasic character. These results suggest a small amount of activation from unbalanced visual motion between horizontal and off-horizontal eye movement phases (see Discussion).

Visual stimulation (with an attentional task) produced clear, largely medial-lateral phase progressions corresponding to a representation of polar angle in the superficial layers of SC (Fig. 4, center column). The stimulation-evoked phase progressions are qualitatively consistent with the progressions evoked by the saccade tasks in each elliptical ROI within each SC. In most participants, we also observed a small rostral-caudal (superior-inferior) tilt of the saccadic eye-movement phase progressions in the lateral-to-medial phase progression. This tilt also corresponded to the tilt in the saccade data. For the saccade task, no consistent phase progressions were elicited in early visual cortex (Fig. S4), indicating that the phase progressions were not associated with visual stimulation alone.

Correlations between eye-movement and visual stimulation topographies

Within the elliptical ROIs for each participant, we observed the saccadic eye movement phases of the three angles of movement to be in alignment with the visual stimulation retinotopy for both left (slope: 0.733, $r = 0.312$, $p = .0052$) and right (slope: 0.928, $r = 0.567$, $p = .0034$) SCs (Fig. 6). Quantitative correlations were significant for five out of ten SCs in individual participants (Fig. S5).

Depth profiles

Laminar depth profiles extended deeper into SC for activity evoked by saccadic eye movements compared to visual stimulation (Fig. 7). The peaks are significantly shifted deeper for eye movement maps compared to visual stimulation maps for both left (shift = 0.9 mm, $p = .0012$) and right (= 0.7 mm, $p = .0002$) SC. At the individual level, data were significant in four out of 10 SC (Fig. S6).

Discussion

We used high-resolution functional MRI to map the polar angle representation of saccadic eye movements within human SC. We found saccades along the superior-inferior visual axis were mapped roughly medial-to-lateral on the anatomy of the SC. Eliciting these maps required a novel paradigm in which participants were cued to make saccades along one of three specified direction axes, and then a smooth pursuit back to the start of the axis. Doing so isolated forward saccades from reverse saccades, while still allowing participants to make many saccades along a controlled set of directions in an experimental session. In addition, we utilized a fixed and symmetric grid of saccade targets to minimize the effects of motion and contrast evoked by retinal slip.

This experimental design was not immediately obvious to us but evolved over time and was only discovered after many failed paradigms (Fig. S1). We found, for example that it was necessary to avoid cascading forward and reverse saccades. If participants are instructed to make a saccade in the opposite direction of the target, these reverse saccades may be similar to an anti-saccade or an eye-movement away from the cued target. Recent fMRI studies in humans have demonstrated markedly decreased activation in SC for luminance driven anti-saccades, with inhibitory signal likely coming from the intraparietal sulcus (Anderson et al., 2008). Also, performing anti-saccades may involve the release of inhibitory control exerted by frontal regions like the dorsal lateral prefrontal cortex (DLPFC) onto the colliculus (Condy et al., 2004), which may further confound SC topography measurements. However, ultimately the gaze must be shifted back to the origin. This could be accomplished by a smooth pursuit back to the origin rather than a saccade. Although monkey electrophysiology has shown that rostral SC neurons have activity in the involvement of smooth pursuits (Basso et al., 2000; Krauzlis et al., 1997), such activity appears similar to that evoked by small amplitude saccades, which should be spatially segregated from the 6° saccades guided by our experimental cues. Further, the vascular noise sources already contaminate measurements around the rostral pole with fMRI measurements. Thus, by using many repeated large amplitude saccades in one direction with a minimal number of smooth pursuits for the return to origin, the SC activity was better associated with the saccades.

We found the representation of saccades in human SC to be in good alignment with the overlying retinotopic topography, consistent with the topography of monkey SC (Schiller and Stryker, 1972; Wurtz and Goldberg, 1972; Basso and May 2017). Further, our previous studies showed that superficial attentional maps in human SC are also in alignment with retinotopic maps (Katyal et al., 2010), revealing that attention, retinotopy, and saccadic eye-movement maps all utilize a similar topography.

The depth profiles show that the saccadic eye movement maps lie 0.7–0.9 mm deeper than visual stimulation maps on both SC. This result is consistent with laminar organization inferred from human SC cytoarchitecture (Qu et al., 2006), from human SC response to visual stimulation (Zhang et al., 2015), and from laminar topography across several species including: guinea pig, cat, galago, macaque, and gray squirrel (May 2006). Profiles showed significant depth separations for only 4/10 colliculi individually, but very strong differences were seen on aggregate. This reflects the noisy and blurry character of our hemodynamic correlates of neural function; many sessions were also needed to resolve differences between the laminar profiles of attention and visual stimulation (Katyal et al., 2010).

The confirmation that saccadic eye movement activity is mediated by the intermediate layers of human SC emphasizes the novelty of our earlier discovery that endogenous attention activity is specifically associated with similar intermediate collicular depths (Katyal and Ress, 2014). Specifically, we found that the activation evoked by attention to a very low contrast stimulus evoked activity that peaked 0.5 mm deeper in SC than the boost in activation evoked by attention to a high-contrast stimulus (Fig. 8). Here, we find that oculomotor activation was deeper yet, ~0.8 mm deeper than that evoked by pure visual stimulation combined with attention. This new result generally supports oculomotor theories of visual spatial attention (Corbetta et al., 1998; Katyal and Ress, 2014; Moore et al., 2003; Rizzolatti et al., 1987) with an emphasis on the relationship between oculomotor substrates and covert spatial attention in the near-absence of sensory input. Our results suggest that deeper layers of the SC might mediate both overt (or exogenous) and covert (or endogenous) orientation of attention. In the presence of a strong visual stimulus, such signals may be projected to the superficial layers to augment the response of visual neurons. During weak visual stimulation, these signals become directly evident in the intermediate layers. Previous results in monkeys support similar involvement of intermediate layer neurons responsive to both visual inputs and eye-movements in covert attention (Hafed et al., 2013, 2011; Ignashchenkova et al., 2004; Krauzlis et al., 2013).

Our experimental stimulus still evoked some activity beyond the contralateral medial-lateral phase progression. In 7 out of 10 colliculi, weaker but significant reverse phase progressions appeared on the ipsi-lateral SC. There are at least three possible reasons for this ipsilaterally evoked activity. First, this activity could be driven by small saccades during the smooth pursuits, particularly as the pursuit approaches the target end-point, and the participant makes a predictive saccade ahead of the pursuit. Second, the ipsilateral activity may be evoked by the observed small correction saccades, as the participant often saccades past the target and corrects by performing one-or-more saccades in the opposite direction to reach fixation upon the target. Third, it may be that the prior targets are still remembered during

the smooth pursuit; activity in monkey SC of both remembered and visually-guided saccade targets has been reported during such smooth pursuits (Dash et al., 2016).

We utilized a fMRI acquisition sequence that pushed the boundaries of 3T subcortical imaging. Our dual-echo spiral sequence (Singh et al., 2017) gave us the higher CNR needed to resolve the intermediate layers of SC. Each session included nearly 2 h of scanning while the participant performed 4000–5000 saccades – a demanding but feasible physical effort. Our scanning methodology should allow further experimentation of visual-motor and multisensory function of the SC. For example, future work could study the topography of auditory signal representations and multisensory integration in the deeper layers of SC, and test the possibility of ocular segregation in the superficial layers. Our experimental paradigm also offers a means to probe the topography of eye movements within cortical regions, such as the frontal eye fields.

There are some limitations to our approach and results. First, saccadic eye movements were not fully controlled. Participants automatically tended to make undesired saccades because of error-correction or prediction. These tendencies broadened the distribution of saccades, and probably generated weaker activation upon the opposite colliculus. Second, visual contrast was not fully balanced as a function of polar angle, resulting in weak activation in early visual areas (Fig. S4). This weak activation probably reflects the small asymmetry of our fixed cue display. Ideally, this display should have been round, but the display slightly clipped along the top and bottom (Fig. 1). Therefore, off-horizontal eye movements would create less visual motion drive than on-horizontal movements. This choice was forced by the 16:9 aspect ratio of our MRI-compatible LCD display, and the need to maximize display visual angle to permit sufficient duty cycle. The biphasic activation may have slightly affected our results, but we believe that their effects were comparatively weak given the quality of our observed correlations. Third, we did observe some variability in the cued eye movements. However, we were only able to obtain reliable, consistent eye-tracking inside the scanner in two participants. The experimental sessions were long (~2 h) and intentionally conducted under minimal light to avoid visual contamination. This forced frequent eye-tracking recalibrations and constricted pupils that did not yield viable eye-tracking in 3 out of the 5 participants. With reliable eye tracking for all participants in the scanner, we could have correlated saccade accuracy and latency with strength of the coherence analyses to measure the effect of task performance on our observed saccadic eye movement maps. Nonetheless, we trained all participants outside of the scanner with high-quality eye-tracking until they achieved good performance in saccade accuracy and latency. Fourth, we did introduce button-pressing and a discrimination task to the experimental paradigm, which presents some concern because the SC is also has a sensorimotor mapping, as previous human fMRI studies have elicited reach-related responses (Himmelbach et al., 2013; Linzenbold and Himmelbach, 2012). However, the button presses occurred at a high frequency (0.7-s interval) throughout all phases of the task, which is unlikely to present a concern given our comparatively coarse (2.4-s) temporal sample together with our phase-encoding analysis approach. Further, the objects for discrimination (circle or square) were randomized from trial-to-trial, making any differential patterns evoked by this task highly unlikely to emerge in our phase-mapping analysis.

Author Manuscript

Author Manuscript

Author Manuscript

Author Manuscript

Conclusions

In summary, our techniques allowed us to reliably measure the functional topography of saccadic eye movements on the human SC. This required using high-resolution functional MRI to reliably resolve a laminar nucleus of midbrain, as well as a novel experimental paradigm that allowed participants to make many saccades in one principle direction while minimizing visual stimulation confounds. The topography of the vertical eye movement maps was arranged medial-laterally, in register with the retinotopic representation of visual stimulation, and emerged from deeper layers in SC, similar to the organization observed in monkey.

The new results extend a range of recent measurements in human SC that link together visual stimulation, attention, and eye movements (Fig. 8). Previous work has demonstrated the retinotopic organization of visual stimulation in superficial SC (DeSimone et al., 2015; Katyal et al., 2010; Schneider and Kastner, 2005), as well as detailed registration between stimulation and visual attention (Katyal et al., 2010). More interesting, we learned that attention to a high-contrast stimulus (putative exogenous or overt attention) evokes a very superficial boost in activity, whereas attention to a weak, low-contrast stimulus (putative endogenous or covert attention) evokes deeper activity consistent with SC intermediate layer laminae (Katyal and Ress, 2014). Here, we confirm the depth registration of this activity with the neural substrates of saccadic eye movements, adding additional evidence to the hypothesis that covert attention to weak stimuli have a particularly close connection to the substrates of oculomotor activity.

Supplementary Material

Refer to Web version on PubMed Central for supplementary material.

Acknowledgements

References

Adamuk E, 1872 Uber angeborene und erworbene Association von F. C. Donders. Albrecht Von Graefes Arch. Furklinische Exp 18, 153–164. 10.1007/BF02262657.

Anderson EJ, Husain M, Sumner P, 2008 Human intraparietal sulcus (IPS) and competition between exogenous and endogenous saccade plans. NeuroImage 40, 838–851. 10.1016/j.neuroimage. 2007.10.046. [PubMed: 18222708]

Apter JT, 1946 Eye movements following strychninization of the superior colliculus of cats. J. Neurophysiol. 9, 73–86. [PubMed: 21019913]

Basso MA, Krauzlis RJ, Wurtz RH, 2000 Activation and inactivation of rostral superior colliculus neurons during smooth-pursuit eye movements in monkeys. J. Neurophysiol 84, 892–908. [PubMed: 10938315]

Basso MA, May PJ, 2017 Circuits for action and cognition: a view from the superior colliculus. Annu. Rev. Vis. Sci 10.1146/annurev-vision-102016-061234.

Brainard DH, 1997 The psychophysics toolbox. Spatial Vis. 10, 433–436.

Chang DHF, Hess RF, Mullen KT, 2016 Color responses and their adaptation in human superior colliculus and lateral geniculate nucleus. NeuroImage. 10.1016/j.neuroimage.2016.04.067.

Condy C, Rivaud-Péchoux S, Ostendorf F, Ploner CJ, Gaymard B, 2004 Neural substrate of antisaccades: role of subcortical structures. Neurology 63, 1571–1578. [PubMed: 15534238]

Connolly JD, Vuong QC, Thiele A, 2015 Gaze-dependent topography in human posterior parietal cortex. Cereb. Cortex N. Y. N 1991 (25), 1519–1526. 10.1093/cercor/bht344.

Corbetta M, Akbudak E, Conturo TE, Snyder AZ, Ollinger JM, Drury HA, Linenweber MR, Petersen SE, Raichle ME, Van Essen DC, Shulman GL, 1998 A common network of functional areas for attention and eye movements. Neuron 21, 761–773. [PubMed: 9808463]

Cynader M, Berman N, 1972 Receptive-field organization of monkey superior colliculus. J. Neurophysiol 35, 187–201. [PubMed: 4623918]

Dash S, Nazari SA, Yan X, Wang H, Crawford JD, 2016 Superior colliculus responses to attended, unattended, and remembered saccade targets during smooth pursuit eye movements. Front. Syst. Neurosci 10 (34). 10.3389/fnsys.2016.00034.

de Weijer AD, Mandl RCW, Sommer IEC, Vink M, Kahn RS, Neggers SFW, 2010 Human fronto-tectal and fronto-striatal-tectal pathways activate differently during anti-saccades. Front. Hum. Neurosci 4 (41). 10.3389/fnhum.2010.00041.

DeSimone K, Viviano JD, Schneider KA, 2015 Population receptive field estimation reveals new retinotopic maps in human subcortex. J. Neurosci. Off. J. Soc. Neurosci 35, 9836–9847. 10.1523/JNEUROSCI.3840-14.2015.

Donders FC, 1872 Ueber angeborene und erworbene Association. Albrecht Von Graefes Arch. Für Ophthalmol. 18, 153–164. 10.1007/BF02262657.

Feldon P, Kruger L, 1970 Topography of the retinal projection upon the superior colliculus of the cat. Vis. Res 10, 135–143. [PubMed: 5440778]

Fuchs AF, Kaneko CR, Scudder CA, 1985 Brainstem control of saccadic eye movements. Annu. Rev. Neurosci 8, 307–337. 10.1146/annurev.ne.08.030185.001515. [PubMed: 3920944]

Furlan M, Smith AT, Walker R, 2015 Activity in the human superior colliculus relating to endogenous saccade preparation and execution. J. Neurophysiol 114, 1048–1058. 10.1152/jn.00825.2014. [PubMed: 26041830]

Glover GH, 1999 Simple analytic spiral K-space algorithm. Magn. Reson. Med 42, 412–415. [PubMed: 10440968]

Glover GH, Lai S, 1998 Self-navigated spiral fMRI: interleaved versus single-shot. Magn. Reson. Med 39, 361–368. [PubMed: 9498591]

Hafed ZM, Chen C-Y, 2016 Sharper, stronger, faster upper visual field representation in primate superior colliculus. Curr. Biol. CB 26, 1647–1658. 10.1016/j.cub.2016.04.059. [PubMed: 27291052]

Hafed ZM, Lovejoy LP, Krauzlis RJ, 2013 Superior colliculus inactivation alters the relationship between covert visual attention and microsaccades. Eur. J. Neurosci 37, 1169–1181. 10.1111/ejn.12127. [PubMed: 23331638]

Hafed ZM, Lovejoy LP, Krauzlis RJ, 2011 Modulation of microsaccades in monkey during a covert visual attention task. J. Neurosci. Off. J. Soc. Neurosci 31, 15219–15230. 10.1523/JNEUROSCI.3106-11.2011.

Himmelbach M, Linzenbold W, Ilg UJ, 2013 Dissociation of reach-related and visual signals in the human superior colliculus. NeuroImage 82, 61–67. 10.1016/j.neuroimage.2013.05.101. [PubMed: 23727531]

Iglesias JE, Van Leemput K, Bhatt P, Casillas C, Dutt S, Schuff N, Truran-Sacrey D, Boxer A, Fischl B, Alzheimer's Disease Neuroimaging Initiative, 2015 Bayesian segmentation of brainstem structures in MRI. NeuroImage 113, 184–195. 10.1016/j.neuroimage.2015.02.065. [PubMed: 25776214]

Ignashchenkova A, Dicke PW, Haarmeier T, Thier P, 2004 Neuron-specific contribution of the superior colliculus to overt and covert shifts of attention. Nat. Neurosci 7, 56–64. 10.1038/nn1169. [PubMed: 14699418]

Katyal S, Greene CA, Ress D, 2012 High-resolution functional magnetic resonance imaging methods for human midbrain. J. Vis. Exp. JoVE, e3746 10.3791/3746. [PubMed: 22617680]

Katyal S, Ress D, 2014 Endogenous attention signals evoked by threshold contrast detection in human superior colliculus. J. Neurosci. Off. J. Soc. Neurosci 34, 892–900. 10.1523/JNEUROSCI. 3026-13.2014.

Katyal S, Zughni S, Greene C, Ress D, 2010 Topography of covert visual attention in human superior colliculus. J. Neurophysiol 104, 3074–3083. 10.1152/jn.00283.2010. [PubMed: 20861435]

Khan R, Zhang Q, Darayan S, Dhandapani S, Katyal S, Greene C, Bajaj C, Ress D, 2011 Surface-based analysis methods for high-resolution functional magnetic resonance imaging. Graph. Models, Computational Modeling in Imaging Sciences 73, 313–322. 10.1016/j.gmod.2010.11.002.

Konen CS, Kastner S, 2008 Representation of eye movements and stimulus motion in topographically organized areas of human posterior parietal cortex. J. Neurosci. Off. J. Soc. Neurosci 28, 8361–8375. 10.1523/JNEUROSCI.1930-08.2008.

Krauzlis RJ, Basso MA, Wurtz RH, 1997 Shared motor error for multiple eye movements. Science 276, 1693–1695. [PubMed: 9180078]

Krauzlis RJ, Lovejoy LP, Zeenon A, 2013 Superior colliculus and visual spatial attention. Annu. Rev. Neurosci 36, 165–182. 10.1146/annurev-neuro-062012-170249. [PubMed: 23682659]

Krebs RM, Woldorff MG, Tempelmann C, Bodammer N, Noesselt T, Boehler CN, Scheich H, Hopf J-M, Duzel E, Heinze H-J, Schoenfeld MA, 2010 High-field FMRI reveals brain activation patterns underlying saccade execution in the human superior colliculus. PLoS One 5, e8691 10.1371/journal.pone.000869. [PubMed: 20084170]

Li T-Q, Takahashi A, Wang Y, Mathews V, Glover GH, 2006 Dual-echo spiral in/in acquisition method for reducing magnetic susceptibility artifacts in blood-oxygen-level-dependent functional magnetic resonance imaging. Magn. Reson. Med 55, 325–334. [PubMed: 16408267]

Linzenbold W, Himmelbach M, 2012 Signals from the deep: reach-related activity in the human superior colliculus. J. Neurosci. Off. J. Soc. Neurosci 32, 13881–13888. 10.1523/JNEUROSCI. 0619-12.2012.

May PJ, 2006 The mammalian superior colliculus: laminar structure and connections. Prog. Brain Res 151, 321–378. 10.1016/S0079-6123(05)51011-2. [PubMed: 16221594]

Meredith MA, Stein BE, 1990 The visuotopic component of the multisensory map in the deep laminae of the cat superior colliculus. J. Neurosci 10, 3727–3742. [PubMed: 2230957]

Mohler CW, Wurtz RH, 1976 Organization of monkey superior colliculus: intermediate layer cells discharging before eye movements. J. Neurophysiol 39, 722–744. [PubMed: 823302]

Moore T, Armstrong KM, Fallah M, 2003 Visuomotor origins of covert spatial attention. Neuron 40, 671–683. [PubMed: 14622573]

Nestares O, Heeger DJ, 2000 Robust multiresolution alignment of MRI brain volumes. Magn. Reson. Med 43, 705–715. [PubMed: 10800036]

Qu J, Zhou X, Zhu H, Cheng G, Ashwell KWS, Lu F, 2006 Development of the human superior colliculus and the retinocollicular projection. Exp. Eye Res 82, 300–310. 10.1016/j.exer. 2005.07.002. [PubMed: 16125175]

Ress D, Glover GH, Liu J, Wandell B, 2007 Laminar profiles of functional activity in the human brain. NeuroImage 34, 74–84. 10.1016/j.neuroimage.2006.08.020. [PubMed: 17011213]

Rizzolatti G, Riggio L, Dascola I, Umilta C, 1987 Reorienting attention across the horizontal and vertical meridians: evidence in favor of a premotor theory of attention. Neuropsychologia 25, 31–40. [PubMed: 3574648]

Robinson DA, 1972 Eye movements evoked by collicular stimulation in the alert monkey. Vis. Res 12, 1795–1808. [PubMed: 4627952]

Schiller PH, Stryker M, 1972 Single-unit recording and stimulation in superior colliculus of the alert rhesus monkey. J. Neurophysiol 35, 915–924. [PubMed: 4631839]

Schluppeck D, Glimcher P, Heeger DJ, 2005 Topographic organization for delayed saccades in human posterior parietal cortex. J. Neurophysiol 94, 1372–1384. 10.1152/jn.01290.2004. [PubMed: 15817644]

Schneider KA, Kastner S, 2009 Effects of sustained spatial attention in the human lateral geniculate nucleus and superior colliculus. J. Neurosci. Off. J. Soc. Neurosci 29, 1784–1795. 10.1523/JNEUROSCI.4452-08.2009.

Schneider KA, Kastner S, 2005 Visual responses of the human superior colliculus: a high-resolution functional magnetic resonance imaging study. J. Neurophysiol 94, 2491–2503. 10.1152/jn. 00288.2005. [PubMed: 15944234]

Sereno MI, Pitzalis S, Martinez A, 2001 Mapping of contralateral space in retinotopic coordinates by a parietal cortical area in humans. Science 294, 1350–1354. 10.1126/science.1063695. [PubMed: 11701930]

Singh V, Pfeuffer J, Zhao T, Ress D, 2017 Evaluation of spiral acquisition variants for functional imaging of human superior colliculus at 3T field strength. Magn. Reson. Med 10.1002/mrm. 26845.

Sparks DL, Hartwich-Young R, 1989 The deep layers of the superior colliculus. Rev. Oculomot. Res 3, 213–255. [PubMed: 2486324]

Sparks DL, Holland R, Guthrie BL, 1976 Size and distribution of movement fields in the monkey superior colliculus. Brain Res. 113, 21–34. [PubMed: 821585]

Sparks DL, Jay MF, 1986 The functional organization of the primate superior colliculus: a motor perspective. Prog. Brain Res 64, 235–241. 10.1016/S0079-6123(08)63418-4. [PubMed: 3726145]

Sprague JM, Meikle TH, 1965 The role of the superior colliculus in visually guided behavior. Exp. Neurol 11, 115–146. [PubMed: 14272555]

Wade A, Brewer A, Rieger J, Wandell B, 2002 Functional measurements of human ventral occipital cortex: retinotopy and colour. Philos. Trans. R. Soc. Lond. B. Biol. Sci 357, 963–973. [PubMed: 12217168]

Wandell BA, Chial S, Backus BT, 2000 Visualization and measurement of the cortical surface. J. Cogn. Neurosci 12, 739–752. [PubMed: 11054917]

Wurtz RH, Albano JE, 1980 Visual-motor function of the primate superior colliculus. Annu. Rev. Neurosci 3, 189–226. 10.1146/annurev.ne.03.030180.001201. [PubMed: 6774653]

Wurtz RH, Goldberg ME, 1972 Activity of superior colliculus in behaving monkey. IV. Effects of lesions on eye movements. J. Neurophysiol 35, 587–596. [PubMed: 4624742]

Xu G, Pan Q, Bajaj CL, 2006 Discrete surface modelling using partial differential equations. Comput. Aided Geom. Des 23, 125–145. 10.1016/j.cagd.2005.05.004. [PubMed: 19830268]

Yushkevich PA, Piven J, Hazlett HC, Smith RG, Ho S, Gee JC, Gerig G, 2006 User-guided 3D active contour segmentation of anatomical structures: significantly improved efficiency and reliability. NeuroImage 31, 1116–1128. 10.1016/j.neuroimage.2006.01.015. [PubMed: 16545965]

Zhang P, Zhou H, Wen W, He S, 2015 Layer-specific response properties of the human lateral geniculate nucleus and superior colliculus. NeuroImage 111, 159–166. 10.1016/j.neuroimage. 2015.02.025. [PubMed: 25703830]
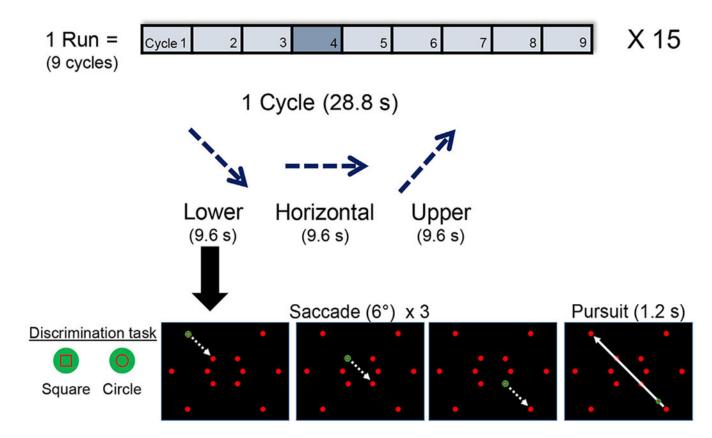
Fig. 1.
Participants performed visually-guided saccades to measure the polar-angle representation of saccades in SC. In each session, activity from one SC was measured by having participants perform saccades toward a single hemifield (right shown here) along a particular polar angle. The stimulus screen showed a static grid of 12 red dots with one target dot turned green to indicate the saccade target. Participants made three 6° saccades along the current polar angle, after which a 1.2-s visually-guided smooth pursuit was made back to the origin along that axis. Upon fixation onto target dots and during the smooth pursuit, participants performed an object discrimination task (square or circle) to keep attention engaged and improve the reliability of eye movements. In each 28.8-s cycle, the vertical component of the saccades progressed through three polar angles: −45° (lower), 0° (horizontal), and +45° (upper). Each session consisted of 15–4.5-min runs, each of which included 9 cycles. (See Fig. S1 for evolution of task design).
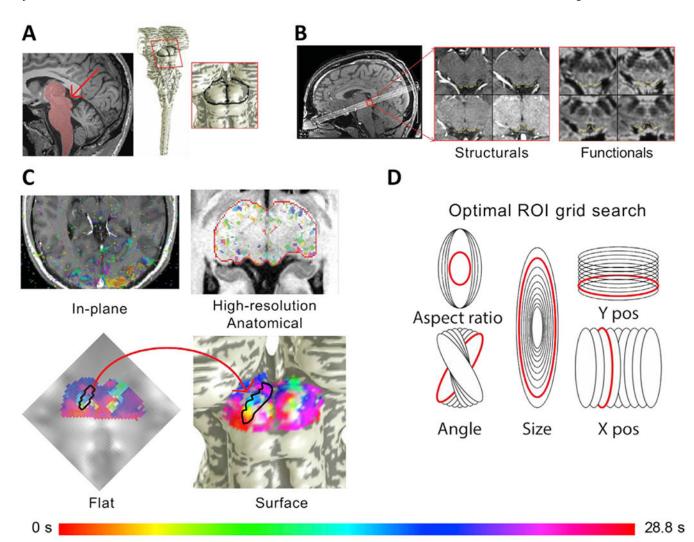
Fig. 2.
SC image acquisition, segmentation, surface projection, and flat maps allowed data visualization to elucidate phase progressions, and optimal selection of ROIs delineating saccadic eye movement representations. **A**. High-resolution (0.7 mm) T1 anatomical images were used to segment the brainstem and create surface models for each participant. The surface maps allowed visualization of the posterior view of the midbrain and SC. **B**. Eight quasi-axial slices through the SC were acquired. In-plane T1 structural slices with the same slice prescription as functional data were obtained before and after collection of functional runs to facilitate registration to high-resolution T1 anatomical. **C**. Functional data were fit with sinusoids and the best fitting phases for each voxel were transformed onto the high-resolution anatomical volume, which could then be projected onto the surface by depth averaging. The depth-averaged functional data were also visualized and analyzed on a 2D projection. **D**. In the flattened view, thousands of elliptical ROIs were generated by manipulating 5 elliptical parameters. The ellipse that best fit the optimization criteria was visualized in the flat view to check for accuracy and then transformed into the volume and the surface model.
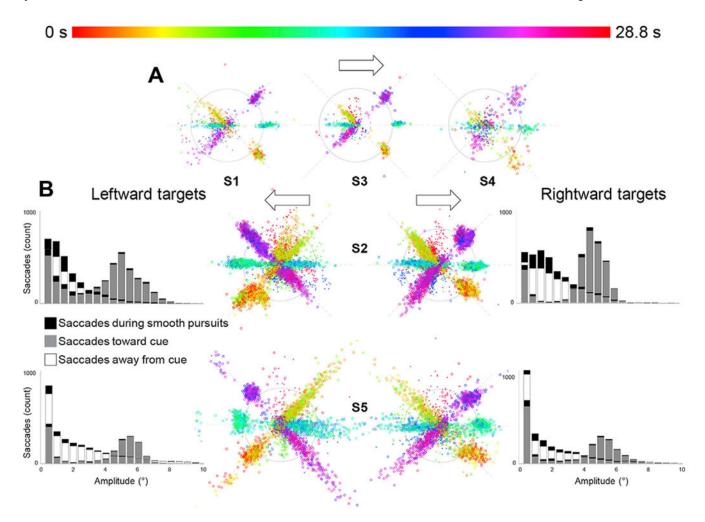
Fig. 3.
Eye tracking confirmed the reliability of participant's eye movements. **A.** Data from three participants show saccades during a training session outside of the scanner. Polar plots show the polar angle and eccentricity of each saccade detected, as well as the corresponding time during the cycle, represented as a color from the HSV color map. **B.** Data from two participants during fMRI acquisition inside the scanner also show reliable eye movements during both leftward and rightward sessions. Histograms show eye movement amplitudes of $6.29° \pm 1.95°$ in the cued direction (shown in gray). Long tailed distributions in the opposite direction (white) were also observed (median: $0.8°$, mean: $3.07° \pm 3.19°$). Eye movments made during smooth pursuits were isolated but still shown here in the polar plots (smaller "x" marks) and the histograms (black fills). (See also Fig. S2 for quantification of behavioral task performances).
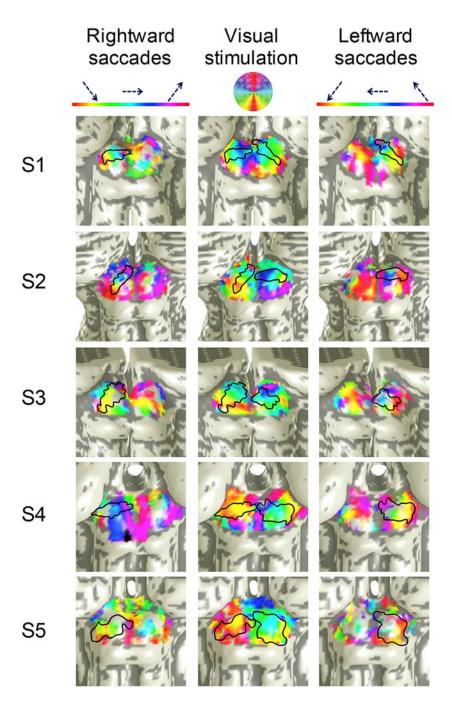
Fig. 4.
Saccadic eye movements along the superior-inferior visual field were mapped medial-laterally on the contralateral SC in five participants. From left to right, the columns of SC surfaces show phase progressions of rightward saccades (left SC), retinotopic mappings, and leftward saccades (right SC). Regions outlined in black show the optimally defined elliptical ROIs on each SC. The elliptical ROIs are also shown on the retinotopy for comparison. (See Fig. S4 for cortical analyses). Note that the color map for the polar-angle retinotopy overlay has been adjusted to match that used for the saccade experiments.
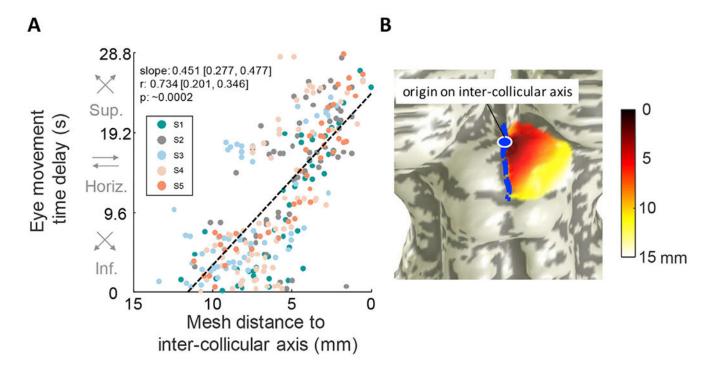
Fig. 5.
Saccadic eye-movement phase increases medially, revealing saccades made superiorly are mapped medially. **A**. The phase of all active vertices ($p < .2$) is plotted against mesh distance from inter-collicular axis for all participants combined, revealing the lateral-medial mapping of eye-movements along the inferior-superior visual axis. Correlation metrics are listed, with 68% confidence interval ranges of slope and correlation values listed, as well as bootstrapped p-values. **B**. Representative participant illustrates mesh distance on a surface SC (data from participant S2). The mesh distance was computed from a vertex along the inter-collicular axis. Data are pooled from all participants and all sessions, totaling 6 sessions from the left SC and 6 sessions from the right SC. (See Fig. S3 for individual participant correlations).
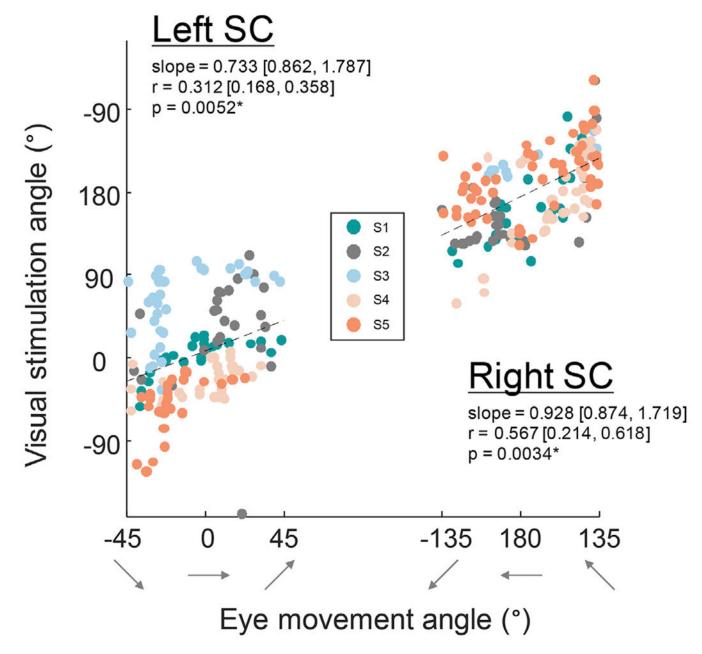
Fig. 6.
Retinotopic organization of superficial layers of SC corresponded with phase progressions of the deeper saccadic eye movement maps. Significant correlations were found for both left and right SCs collapsed across all participants, indicating that these two maps are in alignment. Correlation metrics are listed, with 68% confidence intervals for slope and correlation, as well as bootstrapped p-values. (See Fig. S5 for individual participant's correlations).
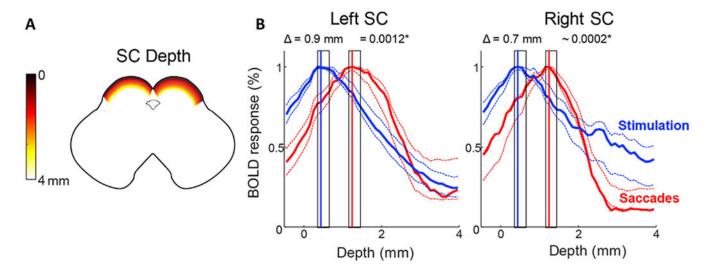
Fig. 7.
Saccadic eye movement maps lie deeper in SC than visual stimulation maps. **A**. Graphic illustrating depth of SC in a horizontal cross section. **B**. Laminar depth profiles for both left and right SC show the activity evoked by saccades (red) lies deeper in SC than activity evoked by visual stimulation (blue). Data are combined across all 5 participants for left and right SC. Dotted lines represent 68% confidence intervals bootstrapped across all runs and participants. The peak is significantly shifted deeper for saccades for both left and right SC (shaded rectangles show bootstrapped 68% confidence intervals for centroid calculations). (See Fig. S6 for individual participant depth profiles).
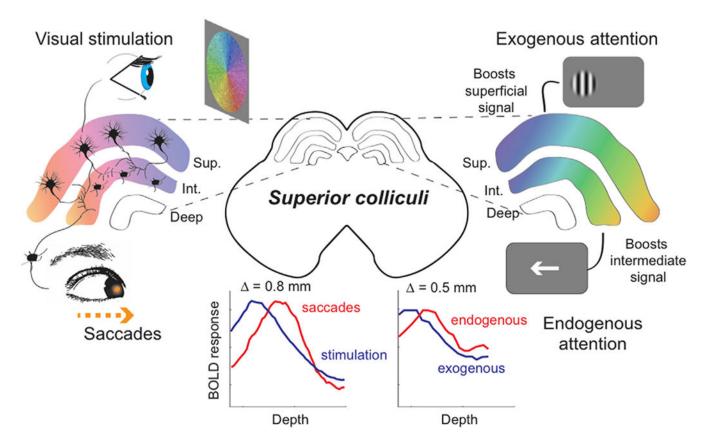
Fig. 8.
Our results link together topography and laminar structure to strengthen the oculomotor theory of attention within the superior colliculus. The panels on the left show that the superficial layers receive direct retinal stimulation, and the intermediate layers drive saccadic eye movements. When attention is engaged (right side), the boost in signal is represented by the increase in color saturation as compared to the left side. The colliculus on the right depicts the effects of exogenous and endogenous attention on the activity of the SC. Exogenous attention boosts the signal within the superficial (Sup.) layers, whereas endogenous attention boosts activity within the intermediate (Int.) layers of SC. The traces on the lower left summarize our depth profiles studied in this paper. The traces on the lower right panel summarize our previous work revealing that endogenous attention gains are observed ~0.5 mm deeper than those evoked by exogenous attention gains (Katyal and Ress, 2014). The color overlays also illustrate the alignment of topographic maps across the laminae.